Eur. Phys. J. C 33, 397–408 (2004)
Digital Object Identifier (DOI) 10.1140/epjc/s2004-01590-2

THE EUROPEAN PHYSICAL JOURNAL C

Leptoproduction of ϱ mesons within Regge approach

S.I. Manayenkov[a]

Petersburg Nuclear Physics Institute, Russian Academy of Science, Gatchina, St.Petersburg district, 188300, Russia

Received: 18 September 2003 / Revised version: 17 December 2003 /
Published online: 13 February 2004 –

Abstract. A model describing the leptoproduction of ϱ mesons is considered. For the amplitude of the photon dissociation into a $q\bar{q}$ pair, the light-cone wave function is used. Scattering of the colorless $q\bar{q}$ pair off the nucleon is computed within reggeon exchange phenomenology. The transition of the scattered quark and antiquark into the final ϱ meson is treated with the aid of the parton–hadron duality concept. Numerical calculations of $R = \sigma_{\rm L}/\sigma_{\rm T}$ and r^{04}_{00} describe the world data at $Q^2 < 4\,{\rm GeV}^2$ rather reasonably. The calculations of the ϱ meson spin density matrix show that the computed matrix elements except r^{04}_{00} are in good agreement with the available experimental data at Q^2 up to $8\,{\rm GeV}^2$ and the total mass of the γp system greater than 4 GeV. The Regge phenomenology predictions at the highest experimentally available energies agree with both the HERA data and calculations performed within the perturbative QCD approach even for very high Q^2 ($\sim$ 10–20 GeV^2). The predicted scale of the S-channel helicity non-conservation is in reasonable agreement with the experimental data.

1 Introduction

Diffractive vector-meson photoproduction and leptoproduction in electron, positron, and muon beams have been under investigation for many years (see, for instance, the reviews in [1,2]). The vector-meson-dominance model and generalized vector-meson-dominance model were used to describe the available data at low photon virtuality Q^2 [1,2]. The S-channel helicity conservation (SCHC) was found to be a good approximation valid within a 10% accuracy. In the last decade, the interest to diffractive vector-meson production in deep inelastic scattering of high energy leptons off nucleons rose since perturbative QCD (pQCD) was argued to be applicable for the description of hard diffraction. The most intriguing predictions were maybe those [3–7] made in the framework of pQCD that the differential cross section of the diffractive vector-meson production in scattering of virtual photons from the proton at high $Q^2 + m_V^2$ and small Bjorken variable x is proportional to the square of the gluon distribution $G^2(x, Q^2)$ (more precisely the skewed gluon distribution for non-forward meson production) in the target, where m_V is the vector-meson mass, $V = \varrho$, ω, Φ, J/Ψ etc. The spin-dependent gluon distribution can be also extracted from experimental data on the double spin asymmetry in the reaction

$$\gamma^* + p \to V + p' \tag{1}$$

at high $Q^2 + m_V^2$ and small x [8]. It was shown that the hard diffraction (1) can be described in the framework of perturbative QCD even for the low momentum-transfer squared t between the incoming and outgoing proton if the hard scale $Q^2 + m_V^2$ is large enough (see below). The photon four-momentum is denoted by q, $Q^2 = -q^2 > 0$, v is the vector-meson momentum, $v^2 = m_V^2$, $t = \Delta^2$, $\Delta = v - q = p - p'$, where p/p' denotes the momentum of the incident/outgoing proton ($p^2 = (p')^2 = M^2$).

It is well known that the process (1) has three stages if the photon–proton center-of-mass (CM) collision energy W is high enough ($W^2 = S_{\gamma p} = (q+p)^2$). First, the virtual photon splits into a quark–antiquark pair. According to the uncertainty principle, the lifetime of the $q\bar{q}$ fluctuation τ_γ (we take $\hbar = c = 1$) is [4]

$$\tau_\gamma \sim q_+ / \left[Q^2 + M_i^2\right] , \tag{2}$$

where M_i in (2) is the mass of the $q\bar{q}$ pair, $q_\pm = (q_0 \pm q_z)/\sqrt{2}$, and q_0 and $q_z = \sqrt{q_0^2 + Q^2}$ denote the energy and three-momentum of the virtual photon, respectively (we consider the center-of-mass $\gamma^* p$ system in which the Z-axis is directed along the photon three-momentum and the X-axis belongs to the lepton scattering plane). If $Q^2 > M_i^2$ formula (2) in the rest frame of the target for the ϱ meson production can be rewritten [4] as

$$\tau_\gamma \sim 1/[Mx] , \tag{3}$$

where $x = Q^2/(2p \cdot q)$ is the famous Bjorken variable. Second, scattering of the quark–antiquark pair on the proton at high energies for large $Q^2 + m_V^2$ and small x can be described in the double-logarithmic approximation of pQCD through two gluon exchange ladder graphs. As was shown [4] in this approximation the interaction time $\tau_{\rm i}$ is much smaller than τ_γ which means that the $q\bar{q}$ pair is

[a] e-mail: sman@pcfarm.pnpi.spb.ru

prepared long before the interaction with the proton. The dissociation length $l_\gamma = c\tau_\gamma$ is assumed to be much greater than the proton radius r_p being of the order of 1 fm. The third subprocess is the creation of the final vector meson from the scattered quark and antiquark. The formation time for $-t \ll Q^2$,

$$\tau_f \sim q_+/M_f^2\,, \tag{4}$$

is greater than the photon dissociation time [4], hence it is much greater than the interaction time and the formation length $l_\mathrm{f} = c\tau_\mathrm{f} \gg r_p$. The mass of the quark–antiquark pair after scattering on the proton is denoted in (4) by M_f ($M_f \sim M_i$).

The hard scale needed for the applicability of pQCD is usually assumed to be

$$Q_0^2 = (Q^2 + m_V^2)/4\,. \tag{5}$$

But as was argued in [6] the pQCD factorization scales for the production of the vector mesons with the longitudinal and transverse polarizations are

$$Q_\mathrm{L}^2 \sim 0.15(Q^2 + m_V^2), \quad Q_\mathrm{T}^2 \sim 0.07(Q^2 + m_V^2)\,, \tag{6}$$

respectively. This means, strictly speaking, that even the experimental data obtained at the HERA collider for the highest Q^2 correspond to a semiperturbative regime of $q\bar{q}$ scattering off the proton. Nevertheless, numerical calculations of the cross sections are in reasonable agreement with the available data for the region $Q^2 > 4\,\mathrm{GeV}^2$ (see below). Moreover, the calculations [9–11] of the ϱ meson spin density matrix carried out in the pQCD framework for $W = 75\,\mathrm{GeV}$ are in unexpectedly good agreement with the high energy data [12,13] obtained at the HERA collider even for $Q^2 < 1\,\mathrm{GeV}^2$.

We attempt in the present work to describe experimental data on diffractive ϱ meson production at $Q^2 \sim$ a few GeV^2 for low Bjorken variable x using the Regge formalism for the amplitude of $q\bar{q}$ pair scattering off the target. The parameters of the quark–reggeon vertices were obtained in [14] with the aid of the parameters of the nucleon–reggeon vertices found in [15–17] by fitting the experimental data on hadron–nucleon scattering. Exchanges with the pomeron P and secondary reggeons f, ϱ, ω, A_2 are taken into account. We do not restrict ourselves to the one reggeon exchange approximation as in [18] but consider one, two and three reggeon exchanges, besides one and two secondary reggeon exchanges being taken into account only.

This paper is organized as follows. The basic formulae are presented in Sect. 2. The comparison of the calculations with experimental data and the theoretical predictions obtained in the perturbative QCD framework is made in Sect. 3. The most important results are summarized in Sect. 4.

2 Basic formulae for ϱ meson production

First, we are going to recall some kinematic relations. Let ν and $q_\mathrm{lab} = \sqrt{\nu^2 + Q^2}$ be the virtual photon energy and three-momentum in the rest frame of the initial proton (the laboratory system) of which the axes are parallel to those of the CM system. Then the energies of the ϱ meson and the scattered proton in the laboratory system are $E_\varrho = \nu + t/(2M)$, $E_p' = M - t/(2M)$, respectively. The angle between the total three-momentum of the ϱ meson and the photon momentum η can be found from the relation

$$\cos\eta = \frac{2\nu^2 + Q^2 - m_\varrho^2 + t(1+\nu/M)}{\sqrt{\nu^2+Q^2}\sqrt{(2\nu + t/M)^2 - 4m_\varrho^2}}\,, \tag{7}$$

the momentum-transfer squared belonging the interval $|t_\mathrm{min}| < |t| < |t_\mathrm{max}|$ where

$$\begin{aligned} t_{\mathrm{min/max}} = {} & 2M^2 \\ & - \frac{2M^2}{(2M\nu + M^2 - Q^2)} \\ & \times \left\{ (\nu + M)\left(\nu + M - \frac{m_\varrho^2 + Q^2}{2M}\right)\right. \\ & \mp \sqrt{(\nu^2+Q^2)} \\ & \times \left[\nu^2 + Q^2 - (1+\nu/M)\left(m_\varrho^2 + Q^2\right)\right. \\ & \left.\left. + \left(\frac{m_\varrho^2 + Q^2}{2M}\right)^2\right]^{1/2}\right\}. \end{aligned} \tag{8}$$

The formula for the time and longitudinal components of Δ in the laboratory system reads

$$\Delta_0^\mathrm{lab} = \frac{t}{2M}\,, \quad \Delta_Z^\mathrm{lab} = \frac{t(1+\nu/M) - m_\varrho^2 - Q^2}{2\sqrt{\nu^2+Q^2}}\,. \tag{9}$$

The transverse part of the momentum transfer $\mathbf{\Delta}_\mathrm{T}$ will be defined below. The transverse part of any three-vector $\mathbf{b}$ will be denoted $\mathbf{b}_\mathrm{T} = (b_X, b_Y, 0)$. The four-momentum of the photon in the $\gamma^* p$ center-of-mass system is $q = (q_0, q_Z, \mathbf{0})$ where

$$q_0 = \frac{M\nu - Q^2}{W}\,, \quad q_Z = \frac{M\sqrt{\nu^2+Q^2}}{W} = \frac{M}{W} q_\mathrm{lab}\,, \tag{10}$$

with $W^2 = 2M\nu + M^2 - Q^2$. The ϱ meson momentum $v = (v_0, v_Z, \mathbf{v}_\mathrm{T})$ has the components in the CM system $\left(|\mathbf{v}| = \sqrt{v_Z^2 + \mathbf{v}_\mathrm{T}^2}\right)$

$$\begin{aligned} v_0 &= \frac{2M\nu + m_\varrho^2 - Q^2}{2W}\,, \\ |\mathbf{v}| &= \frac{\sqrt{(2M\nu - Q^2 - m_\varrho^2)^2 - 4m_\varrho^2 M^2}}{2W}\,, \\ v_Z &= \frac{W}{2M\sqrt{\nu^2+Q^2}} \end{aligned} \tag{11}$$

$$\times \left[M\nu + t - \frac{M\nu(M^2+m_\varrho^2) - M^2(Q^2-m_\varrho^2)}{W^2} \right],$$

and $\mathbf{v}_\mathrm{T} = \mathbf{\Delta}_\mathrm{T}$, $|\mathbf{v}_\mathrm{T}| = \sqrt{\mathbf{v}^2 - v_Z^2}$. The momentum transfer $\Delta = v - q = (\Delta_0, \Delta_Z, \mathbf{\Delta}_\mathrm{T})$ is given by the relations

$$\Delta_0 = \frac{m_\varrho^2 + Q^2}{2W},$$

$$\Delta_Z = \frac{W}{2M\sqrt{\nu^2+Q^2}} \left[t - \frac{(m_\varrho^2+Q^2)M(\nu+M)}{W^2} \right],$$

$$\mathbf{\Delta}^2 = \mathbf{\Delta}_\mathrm{T}^2 + \Delta_Z^2 = -t + \frac{(m_\varrho^2+Q^2)^2}{4W^2}. \quad (12)$$

If the conditions

$$x \ll 1, \quad \nu \gg M, \quad |t| < M^2 \quad (13)$$

are fulfilled it follows from (12) that both Δ_+ and $2\Delta_+\Delta_-$ are small and we may put $\Delta_+ \approx 0$ in our calculations in the CM system (the precise relation $\Delta_+ = 0$ is valid in the Breit system). Indeed, one has from (12)

$$-\sqrt{2}\Delta_+ = -\Delta_0 - \Delta_Z \approx -t\frac{W}{2M\nu} + \frac{(m_\varrho^2+Q^2)M}{2W\nu}$$
$$\approx -\frac{t}{W} + M^2\frac{(m_\varrho^2+Q^2)}{W^3} \ll |\mathbf{\Delta}_\mathrm{T}|,$$
$$-2\Delta_+\Delta_- \approx \frac{t^2}{W^2} - \frac{t}{W^2}(m_\varrho^2+Q^2) - t_\mathrm{min} \ll \mathbf{\Delta}_\mathrm{T}^2, \quad (14)$$

where $t_\mathrm{min} \approx -M^2(m_\varrho^2+Q^2)^2/W^4 \sim -M^2x^2$, which follows from (8) if (13) are valid. Neglecting Δ_+ one has $t = 2\Delta_+\Delta_- - \mathbf{\Delta}_\mathrm{T}^2 \approx -\mathbf{\Delta}_\mathrm{T}^2 \equiv -\Delta_\mathrm{T}^2$ (we suppose that $\Delta_\mathrm{T}^2 \gg |t_\mathrm{min}|$). If (13) are fulfilled Δ_+^lab in the laboratory system is given by the approximate relation

$$\sqrt{2}\Delta_+^\mathrm{lab} = \Delta_0^\mathrm{lab} + \Delta_Z^\mathrm{lab} \approx \frac{t}{M} - \frac{m_\varrho^2+Q^2}{2\nu}, \quad (15)$$

which follows from (9). Formula (15) shows that the relation $\Delta_+ \approx 0$ which is important for our consideration (see below) is not valid in the laboratory system at $|t| \sim M^2$ even in the limit $\nu \to \infty$. Indeed, $\sqrt{2}\Delta_+^\mathrm{lab} \approx -\Delta_\mathrm{T}\sqrt{-t/M^2}$ in this case, hence $|\Delta_+^\mathrm{lab}| \ll \Delta_\mathrm{T}$ if $-t \ll M^2$. This explains why we prefer to calculate all observables in the CM system rather than in the laboratory system.

According to the physical picture described in the Introduction the amplitude of process (1) can be written as a product of three factors:
(i) the amplitude of the photon dissociation into a quark–antiquark pair;
(ii) the amplitude of scattering of the colorless $q\bar{q}$ pair off the proton;
(iii) the amplitude for the scattered quark and antiquark to create the final meson. In the light-cone perturbative theory [19], the photon wave function looks like [4, 19, 20]

$$\Psi_{\lambda,\nu}^{(\mu)}(\mathbf{k}_\mathrm{T}, z) =$$
$$- ee_q\sqrt{z(1-z)}\frac{\bar{u}_\lambda(\mathbf{k}_\mathrm{T}, z)\epsilon^{(\mu)}\cdot\gamma v_\nu(-\mathbf{k}_\mathrm{T}, 1-z)}{z(1-z)Q^2 + m_q^2 + \mathbf{k}_\mathrm{T}^2}, \quad (16)$$

where e is the positron electric charge, $e_q = 2/3$ or $-1/3$ denotes the fractional charge of a quark with flavor $q = u, d$. The light-cone components of the photon, quark and antiquark momenta are respectively $q = (q_+, q_-, \mathbf{0})$, $k_1 = (k_{1+}, k_{1-}, \mathbf{k}_\mathrm{T})$, $k_2 = (k_{2+}, k_{2-}, -\mathbf{k}_\mathrm{T})$. Their components obey the relations $q_- = -Q^2/(2q_+)$, $k_{1+} = zq_+$, $k_{2+} = (1-z)q_+$. Both the quark and antiquark are on mass shell, $k_1^2 = 2k_{1+}k_{1-} - \mathbf{k}_\mathrm{T}^2 = m_q^2$, $k_2^2 = 2k_{2+}k_{2-} - \mathbf{k}_\mathrm{T}^2 = m_q^2$, with m_q being the quark mass. The bispinor $u_\lambda(\mathbf{k}_\mathrm{T}, z)$ ($v_\nu(-\mathbf{k}_\mathrm{T}, 1-z)$) in (16) describes the quark (antiquark) with the helicity $\lambda/2$ ($\nu/2$) in the infinite momentum frame [21]. The product $\epsilon^{(\mu)}\cdot\gamma$ is the scalar product of the Dirac matrices and the photon polarization vector $\epsilon^{(\mu)}$ given by the relations

$$\epsilon^{(\pm1)} = -\frac{1}{\sqrt{2}}[\pm\mathbf{e}_x + \mathrm{i}\mathbf{e}_y], \quad \epsilon^{(0)} = \left(\frac{q_+}{Q}, \frac{Q}{2q_+}, \mathbf{0}\right), \quad (17)$$

where the unit vectors $\mathbf{e}_x$, $\mathbf{e}_y$ are parallel respectively to the X- and Y-axes in the CM system. Formula (16) gives for the transverse polarization of the photon

$$\Psi_{\lambda,\nu}^{(\pm1)}(\mathbf{k}_\mathrm{T}, z) = \quad (18)$$
$$ee_q\frac{\delta_{\lambda,\nu}(1\pm\lambda)m_q - \delta_{\lambda,-\nu}(1-2z\mp\lambda)(\pm k_x + \mathrm{i}k_y)}{\sqrt{2}\left[z(1-z)Q^2 + m_q^2 + \mathbf{k}_\mathrm{T}^2\right]},$$

and $\Psi_{\lambda,\nu}^{(0)}$ for the longitudinal photon polarization looks like

$$\Psi_{\lambda,\nu}^{(0)}(\mathbf{k}_\mathrm{T}, z) = -ee_q\frac{2Q\delta_{\lambda,-\nu}}{Q^2 + M_i^2}, \quad (19)$$

with M_i being the mass of the $q\bar{q}$ pair before scattering

$$M_i^2 = \frac{m_q^2 + \mathbf{k}_\mathrm{T}^2}{z(1-z)}, \quad (20)$$

and $\delta_{j,k}$ denotes the Kronecker symbol. From here on, the limit $m_q \to 0$ will be considered; hence the helicities of the quark and antiquark become Lorentz invariant quantum numbers.

The amplitude $F_{\lambda'\nu'n',\lambda\nu n}$ of $q\bar{q}$ pair scattering off the proton in the hadronic center-of-mass (HCM) system is calculated in the helicity representation where λ, ν, n (λ', ν', n') are the helicities of the incoming (outgoing) quark, antiquark and proton, respectively. The Z-axis of the HCM system is parallel to the photon three-momentum $\mathbf{q}$ and the Y-axis is directed along the three-vector $\mathbf{q}\times\mathbf{\Delta}_\mathrm{T}$ (for more details see [22]). The formulae for the amplitudes of one, two and three reggeon exchanges are given in [14]. Contributions of pomeron and secondary reggeons $\omega(782)$, $\varrho(770)$, $A_2(1320)$ and $f(1270)$ are considered in the present work. The proton reggeon vertex for natural parity exchange looks like [23–26]

$$R_{n'n}(\Delta) = R_S(\Delta^2)\delta_{n',n} + \mathrm{i}R_Y(\Delta^2)(\mathbf{s}\cdot\mathbf{e}_z\times\mathbf{\Delta}_\mathrm{T})_{n'n}, \quad (21)$$

where $\mathbf{e}_z$ is the unit vector along the Z-axis (the photon three-momentum) and $\mathbf{s} = (\sigma_x, \sigma_y, \sigma_z)$ is a set of the Pauli

matrices acting on the proton helicity variables. The functions R_S and R_Y in (21) were chosen in the Gaussian form

$$R_S(\Delta^2) = r_S \exp\{b_S^2 t\}, \quad R_Y(\Delta^2) = r_Y \exp\{b_Y^2 t\}\,, \quad (22)$$

with the parameters r_S, b_S, r_Y, b_Y found in [15–17]. As was demonstrated in [15–17] the differential cross sections and polarizations in elastic hadron–nucleon scattering and charge exchange reactions in fixed-target experiments at beam energies 10 to 100 GeV and $|t| \leq 0.5\,\mathrm{GeV}^2$ can be described rather well with this set of the vertex parameters and parameters of the Regge trajectories. To get the parameters of the quark–reggeon vertices from the nucleon–reggeon vertices, the nucleon was treated in [14] as a three quark system whose spin structure is described by the non-relativistic quark model [27]. This assumes that the constituent quarks are considered. We suppose that the transformation of the current quark and antiquark into the constituent ones occurs due to irradiation of soft gluons and this process does not significantly change the momentum distribution. Hence the momentum distribution of the constituent quark/antiquark before scattering off the proton can be described with the wave functions (18) and (19). The approach used in [18] is close to that considered here but only spectator graphs are taken into account in [18] when only one constituent of the $q\bar{q}$ pair is involved in the interaction with the proton via reggeon exchanges. The vertices used in [18] are not Gaussian and they take effectively into account few reggeon exchanges in spectator graphs. In our approach, non-spectator diagrams when both the quark and antiquark exchange reggeons with the target are taken into consideration.

There is no good light-cone wave function of the ϱ meson in the literature; therefore we make use of the approach proposed in [5] based on the parton–hadron duality. Since the ϱ meson has $J^P = 1^-$ quantum numbers one considers the "open" $q\bar{q}$ pair production by the heavy photon on the proton with $J^P = 1^-$ and a mass within the ϱ meson mass region. This $q\bar{q}$ state ($u\bar{u}$ and $d\bar{d}$) is transformed into ϱ (which decays into two pions practically with the 100% probability), ω mesons and a non-resonant system of pions with $J^P = 1^-$ and a total mass M_f. We suppose that the total angular momentum of the final $q\bar{q}$ system (after scattering off the nucleon) is conserved in transformation of the current quark and antiquark into the final hadrons which assumes the absence of any additional interaction of the $q\bar{q}$ pair with the target in the fragmentation (approximation of independent fragmentation). This assumption is reasonable since the formation length l_f is supposed to be much greater than the nucleon radius. The ratio of the production cross sections of the ω and ϱ mesons is $\sigma_\omega/\sigma_\varrho \sim (e_u + e_d)^2/(e_u - e_d)^2 = 1/9$ since the meson flavor wave functions in the $SU(3)$ scheme are as follows: $\omega = (u\bar{u} + d\bar{d})/\sqrt{2}$, $\varrho = (u\bar{u} - d\bar{d})/\sqrt{2}$. The non-resonant $\pi\pi$ background in the mass region $0.6 < M_f < 0.9\,\mathrm{GeV}$ is typically a few per cents (see for instance [28–30]). Hence one may calculate the spin density matrix of the $q\bar{q}$ system and identify it with the ϱ meson spin density matrix. It follows from the above discussion that the calculations and experimental data on the pion angular distribution would be in better agreement if the background contributions were not subtracted.

Let the momenta of the scattered quark and antiquark be p_1 and p_2. Since the light-cone component Δ_+ of the momentum transfer is negligibly small, then p_{1+} and p_{2+} coincide with the light-cone components of the initial quark and antiquark (k_{1+} and k_{2+}), respectively. The sum of the transverse components of p_1 and p_2 is equal to $\mathbf{\Delta}_\mathrm{T}$, and both the quark and antiquark are on mass shell. Then we come to the following representation of p_1 and p_2:

$$\begin{aligned}
&p_{1+} = zq_+\,, \quad p_{1-} = \frac{m_q^2 + \mathbf{p}_{1\mathrm{T}}{}^2}{2zq_+}\,,\\
&\mathbf{p}_{1\mathrm{T}} = \mathbf{r}_\mathrm{T} + z\mathbf{\Delta}_\mathrm{T}\,,\\
&p_{2+} = (1-z)q_+\,, \quad p_{2-} = \frac{m_q^2 + \mathbf{p}_{2\mathrm{T}}{}^2}{2(1-z)q_+}\\
&\mathbf{p}_{2\mathrm{T}} = -\mathbf{r}_\mathrm{T} + (1-z)\mathbf{\Delta}_\mathrm{T}\,. \qquad (23)
\end{aligned}$$

It follows from (23) that the total mass of the $q\bar{q}$ pair is given by the relation

$$M_f^2 = \frac{m_q^2 + \mathbf{r}_\mathrm{T}^2}{z(1-z)}\,. \quad (24)$$

In the rest frame of the scattered q and $\bar{q}$ (the ϱ meson rest frame) the three-momentum of any parton is equal to $M_f/2$ (when $m_q = 0$). If they are in the state with the total angular momentum $J = 1$, $J_Z = m$ the angular dependence of their wave function χ is described with the Wigner D-function [31]

$$\chi^m_{\alpha\beta} \sim D^{(1)}_{\alpha-\beta,m}(\cos\theta, \phi, 0)\,. \quad (25)$$

The quark/antiquark helicity is denoted in (25) α/β and θ (ϕ) is the polar (azimuthal) angle of the quark momentum. The standard choice of the axes in the ϱ meson rest frame is the following. The Z-axis is opposite to the outgoing proton three-momentum and the Y-axis is normal to the meson production plane (the plane which is formed by the three-vectors $\mathbf{q}$ and $\mathbf{\Delta}$ in the CM system, the Y-axis is aligned along $\mathbf{q}\times\mathbf{\Delta}$). If we represent the relative transverse momentum of the quark $\mathbf{r}_\mathrm{T}$ in the form $r_x = |\mathbf{r}_\mathrm{T}|\cos\varphi$, $r_y = |\mathbf{r}_\mathrm{T}|\sin\varphi$, then one readily gets the relations

$$\phi = \varphi\,, \quad \cos\theta = 2z - 1\,. \quad (26)$$

Let the amplitude of the $q\bar{q}$ pair production with particle momenta p_1, p_2 ($M_f^2 = (p_1 + p_2)^2$) by the virtual photon with helicity μ on the proton with helicity n be $T_{\lambda'\nu'n',\mu n}(Q^2, W, z, \mathbf{r}_\mathrm{T}, \mathbf{\Delta}_\mathrm{T})$, where λ', ν' and n' denote the helicities in the HCM system of the outgoing quark, antiquark and proton, respectively. Then projecting the $q\bar{q}$ state onto the 1^- state ($J_Z = m$) with the aid of the D-functions we get the formula for the amplitude

$$\begin{aligned}
&T_{m\lambda'\nu'n',\mu n}(Q^2, W, M_f^2, t)\\
&= \int D^{*(1)}_{\omega,m}(\cos\theta, \phi, 0)\tilde{T}_{\lambda'\nu'n',\mu n}(Q^2, W, z, \mathbf{r}_\mathrm{T}, \mathbf{\Delta}_\mathrm{T})
\end{aligned}$$

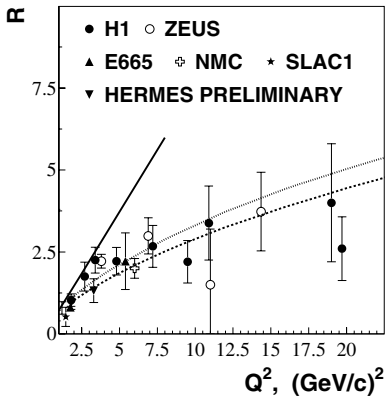

Fig. 1. Comparison of calculated $R = \sigma_{\rm L}/\sigma_{\rm T}$ with high-Q^2 data. The solid line is computed in the Regge approach, the other curves are obtained in [5] within the pQCD framework. To calculate the dotted and dashed curves, MRST99 [36] and CTEQ(5M) [37] gluon distributions are used, respectively. Experimental points show results obtained in electroproduction at DESY by the H1 [12,28], ZEUS [13,32], HERMES (preliminary) [29], at SLAC [35] and in muoproduction by the E665 [33] and NMC [34] collaborations

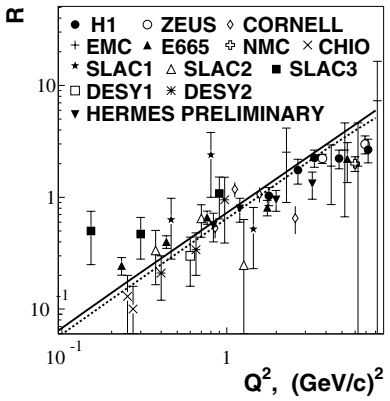

Fig. 2. Comparison of calculation within the Regge approach with experimental data on $R = \sigma_{\rm L}/\sigma_{\rm T}$. The solid and dashed lines are calculated at $W = 45$ and $W = 6\,\mathrm{GeV}$, respectively. Data are obtained at DESY (H1 [12], ZEUS [13], HERMES (preliminary) [29], DESY1 [38], DESY2 [42]), at Cornell [39] and at SLAC (SLAC1 [35], SLAC2 [40], SLAC3 [41]) in ep scattering and also in μp collisions by the E665 [33], NMC [34], EMC [43], and the CHIO [44] collaborations

$$\times\frac{\mathrm{d}\phi\mathrm{d}\cos\theta}{4\pi}$$
$$=\int_0^{2\pi}\frac{\mathrm{d}\varphi}{2\pi}\int_0^1 D^{*(1)}_{\omega,m}(2z-1,\varphi,0)$$
$$\times\tilde{T}_{\lambda'\nu'n',\mu n}(Q^2,W,z,\mathbf{r}_{\rm T},\mathbf{\Delta}_{\rm T})\mathrm{d}z\,, \qquad (27)$$

where D^* denotes the complex conjugate D-function, $\omega = \lambda' - \nu'$. The relations (26) are used in (27). The tilde in (27) reminds the reader that z and $\mathbf{r}_{\rm T}$ are not independent but obey relation (24) since the $q\bar{q}$ pair has a definite mass M_f. The spin density matrix of the $q\bar{q}$ system (of the produced ϱ meson) according to the von Neumann formula looks like

$$\rho^{(\varrho)}_{mm'} = N\sum_{\lambda',\nu',n',k,n,\mu,\mu'} T_{m\lambda'\nu'n',\mu k}\rho^{(\gamma)}_{\mu\mu'}\rho^{(p)}_{kn}T^*_{m'\lambda'\nu'n',\mu' n}\,, \qquad (28)$$

where the normalization factor N can be found from the relation

$$\mathrm{tr}\,\rho^{(\varrho)} = \sum_m \rho^{(\varrho)}_{mm} = 1\,. \qquad (29)$$

The virtual photon density matrix $\rho^{(\gamma)}_{\mu\mu'}$ in the HCM system was taken from [22] and the proton density matrix $\rho^{(p)}_{kn}$ is given by the unit matrix for the unpolarized proton. The standard decomposition of $\rho^{(\gamma)}_{\mu\mu'}$ leads to the decomposition of the vector-meson density matrix $\rho^{(\varrho)}_{mm'}$ into the matrices $r^{(04)}_{mm'}$, $r^{(1)}_{mm'}$, …, $r^{(9)}_{mm'}$ [22].

3 Numerical results and discussion

In this section, we compare the calculation of the spin density matrix with the available experimental data on exclusive ϱ meson production by leptons to establish the W and Q^2 regions where the Regge phenomenology approach is applicable. We start our consideration with the ratio $R = \sigma_{\rm L}/\sigma_{\rm T}$ of the ϱ meson production cross sections with the longitudinal and transverse photons. Figure 1 shows that the high-Q^2 data [12,13,28,29,32–35] are in excellent agreement with the calculations [5] performed within the perturbative quantum chromodynamics framework. The errors shown in Fig. 1 represent the statistical and systematic errors added in quadrature. The same is done for all experimental points shown in the present paper. The difference between the calculations made with the MRST99 [36] and CTEQ(5M) [37] parton distributions in the proton demonstrates the order of magnitude of the pQCD calculation uncertainty. Even if the hard scale is given by relation (5) the pQCD calculations are not to be applicable at $Q^2 < 4\,\mathrm{GeV}^2$ since this assumes that $Q_0^2 \sim 1\,\mathrm{GeV}^2$ for the light meson production. Strictly speaking, the applicability of pQCD for the calculation of the exclusive ϱ meson production even for $Q^2 \sim 10\,\mathrm{GeV}^2$ is questionable [6] since the hard scales $Q^2_{\rm L}$ and $Q^2_{\rm T}$ given by (6) are $\sim 1\,\mathrm{GeV}^2$. Our calculations based on the Regge phenomenology disagree with the available data for $Q^2 > 4\,\mathrm{GeV}^2$, but they are in reasonable agreement with the experimental data at $Q^2 < 4\,\mathrm{GeV}^2$. The calculations both in the pQCD framework and within the Regge approach are performed at the $\gamma^* p$ collision energy $W = 45\,\mathrm{GeV}$. Since the larger part of the low-Q^2 data are obtained for smaller W we calculate the ratio $\sigma_{\rm L}/\sigma_{\rm T}$ for $W = 6\,\mathrm{GeV}$ (the HERMES kinematics) also. We compare the calculations for $W = 6\,\mathrm{GeV}$ (the dashed curve) and $W = 45\,\mathrm{GeV}$ (the solid line) with the data [12, 13, 28, 29, 32–35, 38–44] at $Q^2 < 8\,\mathrm{GeV}^2$ in Fig. 2. As is seen from Fig. 2 the Regge approach calculations with the parameters of the nucleon–reggeon vertices taken from [15–17] and those of the reggeon trajectories found in [15–17, 24, 25] are in reasonable agreement with the available data for $Q^2 < 4\,\mathrm{GeV}^2$. We see also from Fig. 2

that the difference between the solid and dashed curves is about equal to or less than the experimental uncertainties.

It is well known that the measured cross section σ is an admixture of the ϱ meson production cross sections with the longitudinal ($\sigma_{\rm L}$) and transverse photons ($\sigma_{\rm T}$)

$$\sigma = \sigma_{\rm T} + \epsilon\sigma_{\rm L}\,, \tag{30}$$

with ϵ being the ratio of the fluxes of the longitudinal to transverse photons:

$$\epsilon = \frac{1-y-y^2Q^2/(4\nu^2)}{1-y+y^2/2+y^2Q^2/(4\nu^2)} \approx \frac{1-y}{1-y+y^2/2}\,. \tag{31}$$

The lepton mass in formula (31) is put equal to zero, and y is the fraction of the incident lepton energy carried by the photon in the laboratory system ($y = (q\cdot p)/(l\cdot p)$ with l being the lepton four-momentum). If conditions (13) are fulfilled the approximate equality in (31) is valid. Measuring σ at different ϵ but for the same Q^2 and W one can get both $\sigma_{\rm L}(Q^2,W)$ and $\sigma_{\rm T}(Q^2,W)$ and their ratio R. Instead of this approach the hypothesis that the produced vector meson has the same helicity as the initial virtual photon (the SCHC approximation) is commonly used to get R. Then measuring the density matrix of the produced meson one gets the ratio $R = \sigma_{\rm L}/\sigma_{\rm T}$ from the relation

$$R = \frac{1}{\epsilon}\frac{r^{04}_{00}}{1-r^{04}_{00}}\,. \tag{32}$$

The definition of the matrix elements $r^a_{\alpha\beta}$ can be found elsewhere [22]. To estimate the difference between the true ratio of the cross sections and R obtained with the aid of formula (32), we have calculated R for $W = 6\,\text{GeV}$ applying (32). Both ratios are found to coincide within the 7% accuracy at $Q^2 < 4.5\,\text{GeV}^2$. The same comparison for $W = 45\,\text{GeV}$ shows that the difference between calculations is much less than 1% even for $Q^2 < 8\,\text{GeV}^2$.

We discuss the dependence of the matrix elements of the ϱ meson density matrix on kinematic variables and we start our consideration from those matrix elements which are non-zero in the SCHC approximation. The sensitivity of the matrix elements to the ϱ meson mass is illustrated with Fig. 3a,b for r^{04}_{00} and r^1_{1-1}, respectively. The calculations were performed at the positron beam energy $E_e = 27.5\,\text{GeV}$ and for $y = 0.8$ which correspond to the HERMES kinematic conditions ($W \approx 6\,\text{GeV}$). As is seen from Figs. 3a,b the curves describe the preliminary HERMES data [29] and data from [38, 41, 44] quite well, but there is presumably some discrepancy between the data [35, 42] and the presented computations. We should remark that the Regge phenomenology is applicable to the proton–proton scattering at energies higher than $E_{pp} \sim 10\,\text{GeV}$ which corresponds to $S_{pp} \approx 20\,\text{GeV}^2$. The preliminary HERMES data were obtained at $S_{\gamma p} = W^2 \approx 36\,\text{GeV}^2$ and the W region for the CHIO data was $10 < W < 16\,\text{GeV}$; hence $S_{\gamma p} > 100\,\text{GeV}^2$. The low energy data [35, 38, 41, 42] were obtained at $S_{\gamma p} < 10\,\text{GeV}^2$ (the mean value of W for the data [38, 42] is equal to 2.3 GeV, $\langle W\rangle = 2.8$–$3.14\,\text{GeV}$ for the SLAC data [35, 41]). Hence we should not pretend to describe well the low energy data [35, 38, 41, 42] and even agreement between the calculations under discussion and the data [38, 41] should be considered as an accidental fact (some play of statistics). Another important reason why our calculations do not describe the data at $W \sim 2$–$3\,\text{GeV}$ is as follows. The parameter $c\tau_\gamma$ given by (3) is approximately equal to 1 fm just for $W = 2.3\,\text{GeV}$, $Q^2 = 1\,\text{GeV}^2$ and the condition $c\tau_\gamma \gg r_p$ is not fulfilled (we recall that $c = 1$) which makes our approach invalid.

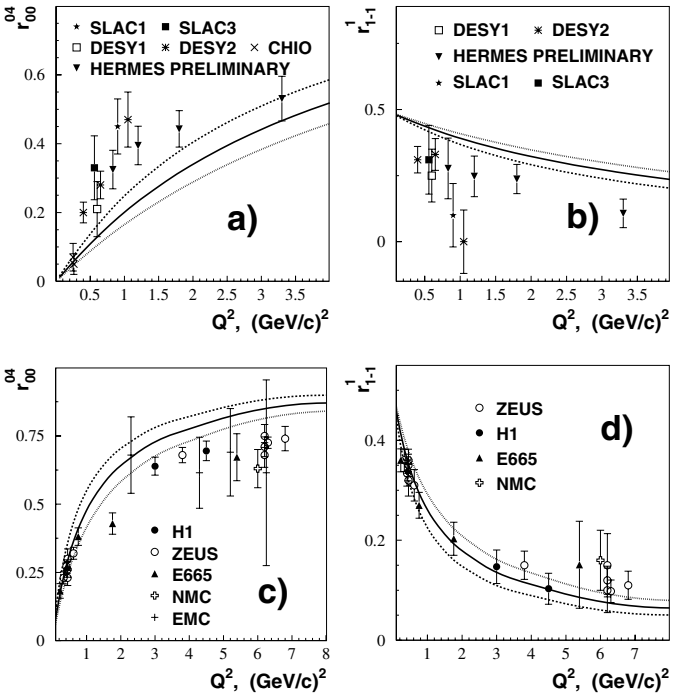

Fig. 3a–d. Dependence of the spin density matrix elements r^{04}_{00} and r^1_{1-1} on Q^2 and ϱ meson mass m_ϱ. The dashed, solid and dotted curves are calculated at $\Delta_{\rm T} = 0$ for $m_\varrho =$ 0.67, 0.77, 0.87 GeV, respectively. All curves in **a** and **b** are computed for the CM energy $W = 6\,\text{GeV}$ and the curves in **c** and **d** are obtained at $W = 45\,\text{GeV}$. Data are from SLAC (SLAC1 [35], SLAC3 [41],) DESY (DESY1 [38], DESY2 [42], HERMES (preliminary) [29], H1 [12], ZEUS [13]), Fermilab (CHIO [44], E665 [33]), and CERN (NMC [34], EMC [43])

The results of the calculations of the matrix elements r^{04}_{00} and r^1_{1-1} for the high energy are displayed in Figs. 3c,d. The curves are computed for $W = 45\,\text{GeV}$ and compared with the data from the H1 [12, 28], ZEUS [13, 32], E665 [33], NMC [34], and EMC [43] collaborations. The data obtained at the HERA collider ($30 < W < 120\,\text{GeV}$) and the fixed-target experiment data ($W \approx 18\,\text{GeV}$ for E665, $7.7 < W < 18\,\text{GeV}$ for NMC, $6 < W < 22.7\,\text{GeV}$ for EMC) are placed together as the W dependence for high energies is rather flat. The calculations in the model under consideration confirm such a dependence (for a more detailed discussion see below).

As is seen from Fig. 3 the difference between the curves obtained for different m_ϱ in any figure is less than the uncertainty of the available data. The parton–hadron duality supposes that the matrix elements are to be averaged over

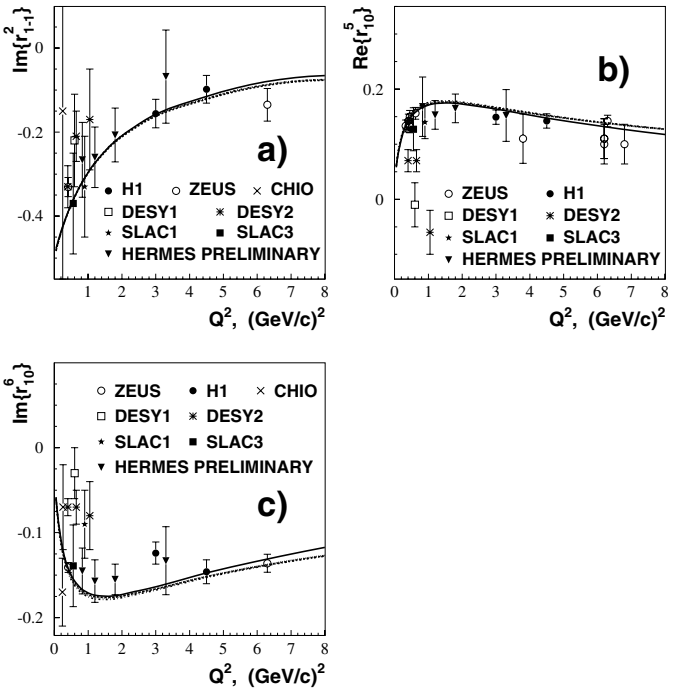

Fig. 4a–c. Dependence of the ϱ meson density matrix elements $\Im\{r^2_{1-1}\}$, $\Re\{r^5_{10}\}$, and $\Im\{r^6_{10}\}$ on Q^2 for different W. The solid, dashed, dotted and dash-dotted curves are calculated for $W = 6$, 13.6, 19.3, and 27.4 GeV at $\Delta_{\rm T} = 0$. Data are obtained at DESY (H1 [12], ZEUS [13], HERMES (preliminary) [29], DESY1 [38], DESY2 [42]), at SLAC (SLAC1 [35], SLAC3 [41]) and by the CHIO collaboration [44]

some ϱ meson mass interval (for example in the region $0.63 < m_\varrho < 0.91$ GeV which was used in the HERMES experiment [29]). But Fig. 3 shows that one can make use of a simplified approach applying the mean value of the ϱ meson mass instead of averaging over some mass region, besides the accuracy of the simplified calculation being not worse than the experimental accuracy. From here on, all our calculations are carried out for $m_\varrho = 0.77$ GeV.

Comparing the curves in Fig. 3a which correspond to the relatively low energy ($W = 6$ GeV) with those in Fig. 3c obtained at $W = 45$ GeV (or the curves in Fig. 3b with the curves in Fig. 3d) we conclude that the behavior of the curves is changed with increasing the center-of-mass energy and the curves describe quite reasonably both the data at $W \approx 6$ GeV and the high energy data ($18 < W < 92$ GeV) for $Q^2 < 4\,\mathrm{GeV}^2$. As was observed experimentally in [13] there is practically no W dependence of r^{04}_{00}, r^1_{1-1} and r^5_{10} between $W = 27.5$ GeV and $W = 92$ GeV for $Q^2 < 6.2\,\mathrm{GeV}^2$. Our calculations confirm this observation. Therefore we may present in Figs. 3c,d the data obtained by H1, ZEUS, E665, NMC, EMC at different (but high) energies together. We see also from a comparison of Figs. 3b,d with Figs. 3a,c that the calculations reproduce the W dependence of r^1_{1-1} even better than that of r^{04}_{00} for Q^2 up to $7\,\mathrm{GeV}^2$.

In the SCHC approximation when only natural parity exchanges in the t-channel are taken into account, the matrix elements r^{04}_{00} and r^1_{1-1} are not independent but they obey the relation

$$1 - r^{04}_{00} - 2r^1_{1-1} = 0\,, \tag{33}$$

which is satisfied within approximately 1.6 standard deviation [13]. This means that Figs. 3a–d show the behavior of one independent matrix element only. Figures 4a,b show the sensitivity of two other independent matrix elements, $\Im\{r^2_{1-1}\}$ and $\Re\{r^5_{10}\}$, to the center-of-mass energy, W. The calculations were performed for the electron beam energy $E_e = 2000$ GeV at $y = 0.01$, 0.05, 0.1, and 0.2 which correspond to the total hadronic masses $W \approx 6$, 13.6, 19.3, and 27.4 GeV. It is easy to see that there is practically no W dependence in the region under discussion where the contribution of the secondary reggeons (ϱ, ω, A_2 and f mesons) could lead to a sensitivity of the density matrix to the center-of-mass energy. For higher energy, where the pomeron contribution to the amplitudes of reaction (1) dominates, the W dependence is to be very smooth also. We do not divide the data into low and high energy parts since $\Im\{r^2_{1-1}\}$ and $\Re\{r^5_{10}\}$ are approximately independent of W. As is seen from Figs. 4a,b, there is unexpectedly excellent agreement of the calculations with the data obtained at the HERA collider by the H1 and ZEUS collaborations. The curves describe well the low energy data [35,38,41,42] on $\Im\{r^2_{1-1}\}$, the data [35,41] agree with the calculations of $\Re\{r^5_{10}\}$; meanwhile, the curves do not describe the data [38, 42] on $\Re\{r^5_{10}\}$. Nevertheless no definite conclusion about the data quality can be made since the Regge phenomenology fails to describe the data at $W < 4$ GeV as was discussed above.

The matrix element $\Im\{r^6_{10}\}$ obeys the relation

$$\Im\{r^6_{10}\} = -\Re\{r^5_{10}\} \tag{34}$$

valid in the SCHC approximation which was checked experimentally with high accuracy [13] (with the statistical and systematic errors equal to 0.005 and 0.013, respectively). In our approach, relation (34) is precise for $\boldsymbol{\Delta}^2_{\rm T} = 0$ and becomes approximate at $t < 0$ with a relative accuracy $\sim$ a few per cents for $|t| \sim 0.1$–$0.2\,\mathrm{GeV}^2$ (typical experimental mean values of $|t|$). It follows from the above discussion that $\Im\{r^6_{10}\}$ does not give any absolutely new information compared with that provided with $\Re\{r^5_{10}\}$. Figure 4c shows a comparison of the calculation performed within the Regge approach with the data on $\Im\{r^6_{10}\}$. The curves presented in Figs. 4b,c obey relation (34). As is seen from Fig. 4c the high energy data [12,13,44] are rather well described with the curves. The difference between calculation and the H1 point at $Q^2 = 3\,\mathrm{GeV}^2$ (about three standard deviations) is probably nothing else than the play of statistics. The low energy data [35, 41] agree reasonably with the presented curves; meanwhile, the data [38, 42] are in disagreement with the calculations. But since the Regge phenomenology loses its applicability for $W < 4$ GeV no definite statements can be formulated.

To characterize the violation of the S-channel helicity, let us define three small dimensionless parameters:

$$\xi_{01} = \frac{|T_{01}|}{\sqrt{|T_{00}|^2 + |T_{11}|^2}}\,,$$

$$\xi_{10} = \frac{|T_{10}|}{\sqrt{|T_{00}|^2 + |T_{11}|^2}}\,,$$
$$\xi_{-11} = \frac{|T_{-11}|}{\sqrt{|T_{00}|^2 + |T_{11}|^2}}\,, \qquad (35)$$

which correspond to the transition of the transverse photon to the longitudinal ϱ meson, the longitudinal photon to the transverse vector meson, and double helicity flip transition, respectively. The symbolic notation $|T_{m\mu}|$ is applied in (35) for the quantities

$$|T_{m\mu}| = \sqrt{\sum_{\lambda',\nu',n',n} |T_{m\lambda'\nu'n',\mu n}|^2}\,, \qquad (36)$$

where the amplitudes $T_{m\lambda'\nu'n',\mu n}$ were defined in (27). It is more convenient from the experimental point of view to introduce the following small parameters [13]:

$$\gamma_{01} = \frac{|r^5_{00}|}{\sqrt{2r^{04}_{00}}}\,,$$
$$\gamma_{10} = \frac{|\Re r^{04}_{10} + \Re r^1_{10}|}{\sqrt{r^{04}_{00}}}\,,$$
$$\gamma_{-11} = \frac{|r^1_{11}|}{\sqrt{2r^1_{1-1}}}\,. \qquad (37)$$

If the value of ϵ defined by (31) is close to unity and the parameters $\xi_{m\mu}$ are small enough, then the parameters $\gamma_{m\mu}$ are approximately equal to $\xi_{m\mu}$ with high accuracy. For the HERA collider kinematics, the relative errors of the relations $\gamma_{m\mu} \approx \xi_{m\mu}$ are less than 10% (typically 1–2%). The parameters ξ_{01}, ξ_{10}, and ξ_{-11} versus Q^2 for different values of t are presented in Figs. 5a–c, respectively. All the quantities $\xi_{m\mu}$ vanish when the transverse momentum transfer, $\Delta_{\rm T}$ is equal to zero. Hence it is very important to know a domain of $-t \approx \Delta^2_{\rm T}$ for which the parameter $\gamma_{m\mu}$ is measured. The experimental values of γ_{01}, γ_{10}, and γ_{-11} are presented in Figs. 5a–c, respectively. The ZEUS data [13] were obtained at $\langle Q^2\rangle = 0.41\,\mathrm{GeV}^2$, $\langle -t\rangle = 0.14\,\mathrm{GeV}^2$ and for $\langle Q^2\rangle = 6.3\,\mathrm{GeV}^2$, $\langle -t\rangle = 0.17\,\mathrm{GeV}^2$, where $\langle Q^2\rangle$ and $\langle -t\rangle$ denote the experimental means of Q^2 and $-t$, respectively. The t region of the data [12] obtained by the H1 collaboration is $0 < -t < 0.5\,\mathrm{GeV}^2$ but $\langle -t\rangle \le 0.2\,\mathrm{GeV}^2$ since the slope parameter, b, of the differential cross section for $1.8 < Q^2 < 10.9\,\mathrm{GeV}^2$ is within the region $5.6 \le b \le 8\,\mathrm{GeV}^{-2}$ [12]. A comparison of the curves with the data shows that they are in agreement.

Owing to the large experimental uncertainty of the modern data we cannot conclude that the available experimental data confirm unambiguously our prediction for the scale of the SCHC violation. The only statement which can be made is that there is no discrepancy between the calculations and the data. More constructive could presumably be a comparison of our calculations with the estimates of the parameters $\xi_{01}, \xi_{10}, \xi_{-11}$ in the framework of perturbative QCD. Indeed, if our approach gives reasonable estimates for the SCHC violation parameters, then they should not

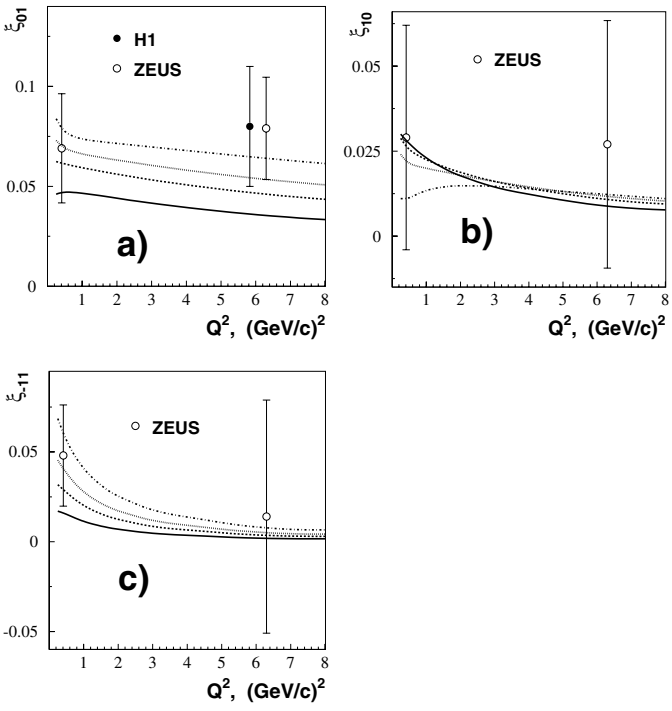

Fig. 5a–c. Comparison of the parameters of SCHC violation ξ_{10}, ξ_{01}, and ξ_{-11} with their experimental estimates γ_{10}, γ_{01} and γ_{-11}. The parameters $\xi_{m\mu}$ and $\gamma_{m\mu}$ are defined by (35) and (37), respectively. The calculations were performed for the HERA collider kinematics at $W = 45\,\mathrm{GeV}$. The solid, dashed, dotted and dash-dotted curves correspond to $|t| = 0.05$, 0.1, 0.15, $0.25\,\mathrm{GeV}^2$. Experimental points are from ZEUS [13] and H1 [12]

disagree with the predictions of pQCD at $Q^2 \approx 4\,\mathrm{GeV}^2$. If we put the formulae (25), (26), (27), (28), and (30) for T_{01}, T_{10}, and T_{-11} of [45] into (35), we get

$$\xi_{01} = \frac{\Delta_{\rm T}/m_\varrho}{\sqrt{1 + Q^2/m^2_\varrho}}\,, \qquad (38)$$

$$\xi_{10} = \frac{\Delta_{\rm T}}{m_\varrho}\frac{Q/m_\varrho}{(1 + Q^2/m^2_\varrho)^{3/2}}\,, \qquad (39)$$

$$\xi_{-11} = \frac{\Delta^2_{\rm T}/m^2_\varrho}{(1 + Q^2/m^2_\varrho)^{3/2}} \qquad (40)$$
$$\times \left[\frac{3}{2}\langle (z-1/2)^2\rangle + \frac{m^2_\varrho}{\mu^2_G}\frac{G(x,\mu^2_G)}{G(x,Q^2_V)}(1 + Q^2/m^2_\varrho)\right]\,,$$

where $Q^2_V \sim (0.1\text{–}0.2)(Q^2 + m^2_\varrho)$ and the parameter $\mu_G \sim 0.7\text{–}1.0\,\mathrm{GeV}$. The quantity $\langle (z-1/2)^2\rangle$ in (40) is the result of averaging $(z-1/2)^2$ over the light-cone wave function of the ϱ meson. The parameter ξ_{-11} has the contribution of non-perturbative effects and therefore contains the gluon density $G(x,\mu^2_G)$ on the non-perturbative scale μ_G which does not depend on Q^2. For rough estimates at $Q^2 \sim 4\,\mathrm{GeV}^2$, we put the ratio $G(x,\mu^2_G)/G(x,Q^2_V)$ equal to unity since $Q^2_V \sim \mu^2_G \sim 1\,\mathrm{GeV}^2$. We make use of the self-evident

inequality $\langle(z-1/2)^2\rangle < 0.25$ and get from (40) the relation

$$\xi_{-11} \leq \frac{\Delta_{\rm T}^2/m_\varrho^2}{(1+Q^2/m_\varrho^2)^{3/2}}\left[\frac{3}{8}+(1+Q^2/m_\varrho^2)\right]. \qquad (41)$$

Formulae (38), (39) and (40) predict that ξ_{01}, ξ_{10} are proportional to $\Delta_{\rm T}$ and $\xi_{-11} \propto \Delta_{\rm T}^2$. As is seen from Fig. 5 the calculated ξ_{01}, ξ_{10}, and ξ_{-11} have a more complicated dependence on $\Delta_{\rm T}$ since one, two and three reggeon exchanges are taken into account which leads to the non-trivial t dependence of $\xi_{m\mu}$. It is easy to see from Figs. 5a–c that $\xi_{01} > \xi_{10} > \xi_{-11}$. This hierarchy in the framework of pQCD was presumably discussed for the first time in [7, 45]. To compare our calculations of the SCHC violation parameters with the prediction of (38), (39) and (41), we consider one reggeon exchange approximation which corresponds to the ladder graph in pQCD. We consider the small $\Delta_{\rm T}$ to have the regime $\xi_{01} \propto \Delta_{\rm T}$, $\xi_{10} \propto \Delta_{\rm T}$, $\xi_{-11} \propto \Delta_{\rm T}^2$. For $Q^2 = 4.5\,{\rm GeV}^2$, $\Delta_{\rm T} = 0.04\,{\rm GeV}$, we get in the Regge phenomenology approach $\xi_{01}^{\rm Regge} = 0.009$. Formula (38) gives $\xi_{01}^{\rm QCD} = 0.018$ which is in reasonable agreement with the value of $\xi_{01}^{\rm Regge}$. For ξ_{10} we get $\xi_{10}^{\rm Regge} = 0.003$ and $\xi_{10}^{\rm QCD} = 0.006$. Both values have the same order of magnitude. For the parameter of the double spin-flip contribution, we have $\xi_{-11}^{\rm Regge} = 0.0001$; meanwhile, formula (41) gives $\xi_{-11}^{\rm QCD} = 0.001$, which is greater by as much as an order of magnitude than in the Regge approach. The pure perturbative contribution to $\xi_{-11}^{\rm QCD}$ (the term proportional to 3/8 in formula (41)) is equal to 0.00004. This value does not disagree sharply with $\xi_{-11}^{\rm Regge}$. Though the QCD estimate has a large theoretical uncertainty due to non-perturbative contributions to ξ_{-11}, nevertheless our estimate of the parameter of the double spin-flip contribution is probably unreliable.

The deviation from the SCHC approximation was experimentally observed in studying the Φ distribution (Φ is the angle between the lepton scattering plane and the meson production plane). It was found [12, 13] that the only non-zero matrix element among those which are to be zero in the SCHC approximation is r_{00}^5. The combinations of the matrix elements most reliably measured in the Φ distribution are as follows:

$$r^5 = 2r_{11}^5 + r_{00}^5\,, \quad r^1 = 2r_{11}^1 + r_{00}^1\,. \qquad (42)$$

They are presented in Figs. 6a,b versus Q^2 for different values of t. The data [12] were obtained for $\langle -t\rangle \sim 0.15$–$0.2\,{\rm GeV}^2$. As is seen from Fig. 6a (dotted and dash-dotted curves) our calculations predict non-zero values for r^5 which are in agreement with the data. The calculated values of r^1 at $Q^2 > 2\,{\rm GeV}^2$ are much smaller than those of r^5 as it follows from a comparison of Fig. 6b with Fig. 6a. The experimental data for r^1 are also in agreement with the presented calculations.

As has been mentioned above the vector-meson electroproduction at high energies and high photon virtualities Q^2 is successfully described within the perturbative QCD framework even for low t. The factorization theorem [46]

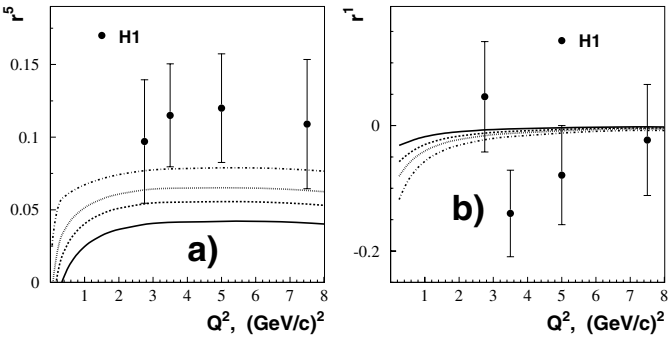

Fig. 6a,b. Comparison of the combinations of matrix elements r_{jk}^a with H1 data. The quantities r^1 and r^5 are defined in (42); the data are from [12]. The calculations are carried out for HERA kinematics at $W = 45\,{\rm GeV}$, solid, dashed, dotted, and dash-dotted curves being computed for $|t| = 0.05$, 0.1, 0.15, $0.25\,{\rm GeV}^2$, respectively

justifies the applicability of pQCD to the amplitude T_{00} of the longitudinally polarized meson production with the longitudinally polarized photon (the spin quantum numbers of the proton are omitted since they are unimportant for our consideration). There is no rigorous proof up to now that the pQCD contribution to the amplitudes $T_{\pm1\pm1}$ of the transverse photon transition to the vector meson with the transverse polarization dominates at high Q^2 but this is presumably the case. It was assumed in [5] that the Q^2 dependence of the gluon density in the proton at small x looks like

$$xG(x,Q^2) = xG(x,Q_0^2)(Q^2/Q_0^2)^\gamma\,, \qquad (43)$$

where Q_0 is a hard scale and γ is the anomalous dimension. Assumption (43) makes the integrals defining the amplitudes T_{11} and T_{-1-1} convergent at $\gamma > 0$ [5, 7]. The gluon distribution of the MRS set of parton densities [47] can be really described with relation (43) with positive γ depending on Q^2. Strictly speaking formula (43) has to be valid at $Q^2 \to 0$; otherwise the integrals for the amplitudes $T_{\pm1\pm1}$ are divergent and the problem of treating end-point singularities arises.

Scattering of the colorless $q\bar{q}$ pair on the proton is described in the pQCD approach through two gluon exchange and the greatest helicity amplitudes (not all of them) of reaction (1) are proportional to the gluon density in the target. It is well known that two gluon exchange corresponds to pomeron exchange. The secondary reggeon contributions are suppressed by a factor $\sim M/W$ at high W. Hence agreement between our calculations and those performed within the pQCD framework can be checked at high energies. We compare our calculations of the spin density matrix elements of the produced ϱ^0 mesons with other theoretical predictions in Fig. 7. Solid lines present results of our calculations performed at $W = 75\,{\rm GeV}$, $-t = 0.15\,{\rm GeV}^2$, and $m_\varrho = 0.77\,{\rm GeV}$. Bullets and circles show the HERA data from H1 and ZEUS [12,13]. The triangles show the results of calculations by Ivanov and Kirschner [7] at $Q^2 = 10\,{\rm GeV}^2$, $-t = 0.167\,{\rm GeV}^2$ and $W = 100\,{\rm GeV}$. Two triangles in every figure correspond to $\gamma = 0.5$ and $\gamma = 0.7$. They coincide

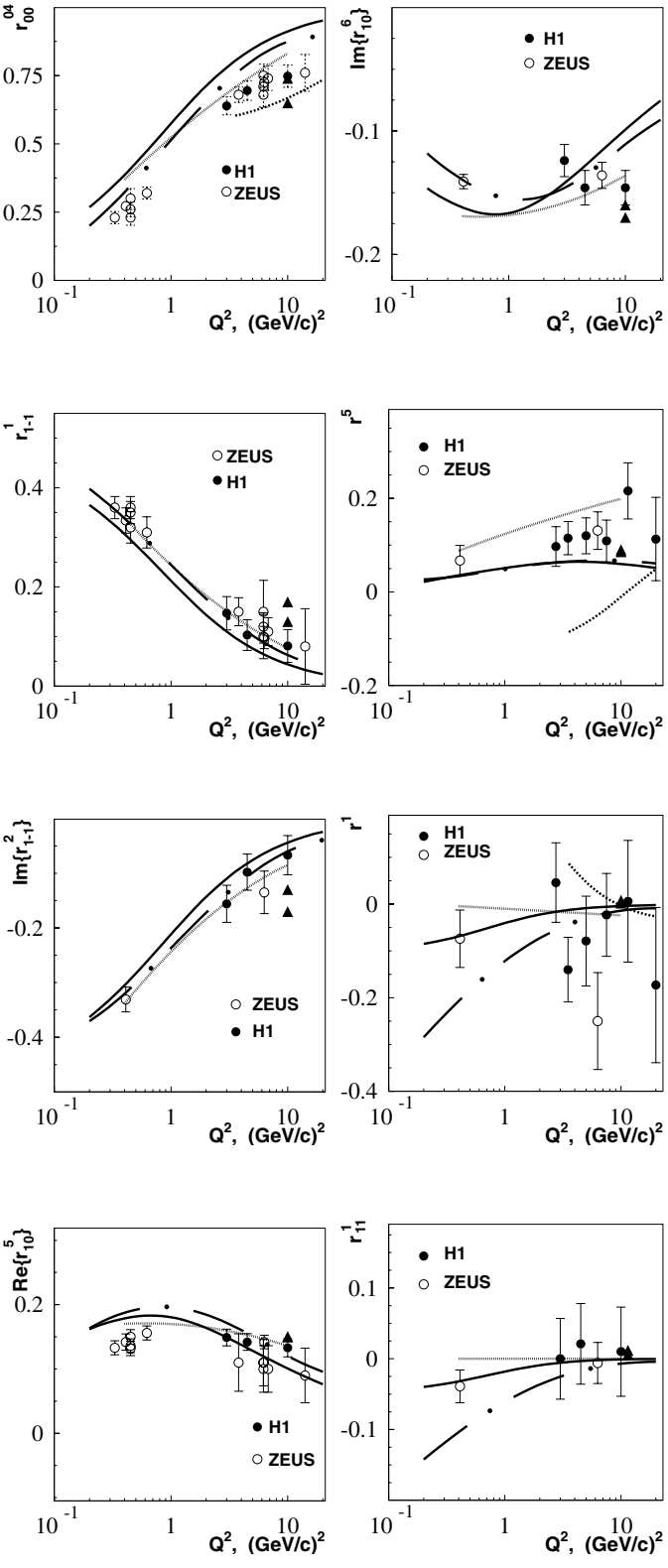

Fig. 7. Comparison of Regge phenomenology predictions with calculations in the pQCD framework. The solid lines show the results of the present work, triangles are obtained by Ivanov and Kirschner [7], dash-dotted curves present calculations by Nikolaev and Ivanov [10,11], dotted curves are computed by Ivanov and Kirschner [49], and dashed curves show the prediction of Royen [50]. Data are from ZEUS [13] and H1 [12]

with each other for $\Re r^5_{10}$, r^5, r^1, and r^1_{11} (r^1 and r^5 are related to r^β_{jk} by (42)). It is easy to see that there is some difference between the triangles and our curves. But this difference could not be considered as the difference between the Regge approach and the perturbative QCD calculations. Indeed, the results of the work [7] are in some disagreement with those by Nikolaev and Ivanov [10,11] made in the perturbative QCD framework also and presented with the dash-dotted curves. The difference is probably related to the approximations used in [7]. Since the heavy photon dissociates into the quark and antiquark with small transverse distance the transition amplitude is sensitive to the vector-meson wave function at small transverse distances. The wave function of the ϱ meson was decomposed in a power series with respect to the transverse distance in [7]. In [10,11], oscillator wave functions [48] having S- and D-wave components were used and numerical calculations of all integrals were performed without any decomposition of the integrands into a power series. One can see that our calculations agree much better with the results by Nikolaev and Ivanov than with the calculations by Ivanov and Kirschner for high Q^2.

The calculations based on perturbative QCD have to use some model for the $q\bar{q}$ component of the wave function of the vector meson. Therefore the results of the calculations become model dependent. The most crucial contributions to the amplitudes are probably the contributions of the so-called end-point singularities which are sensitive to the behavior of the vector-meson wave function at $z \to 0$ and $z \to 1$. They were considered in [49]. The results of the calculations of r^{04}_{00}, r^1, and r^5 made in [49] are presented in Fig. 7 with the dashed curves. Comparison of the dash-dotted and dashed curves shows the order of magnitude of the uncertainty of the modern theoretical calculations performed in the pQCD framework. The dotted curves present the results of computing the spin density matrix elements at HERA collider energies and $-t = 0.138\,\mathrm{GeV}^2$ by Royen [50] in the QCD motivated model. In this work, a phenomenological vertex instead of the gluon distribution $G(x, Q^2)$ is used to describe the interaction of two gluons with quarks in the proton. The vertex function instead of the wave function is used in [50] to describe the transition of the $q\bar{q}$ pair into the ϱ^0 meson, the helicity structure of the vertex being given by the Dirac matrices γ_μ. As is seen from Fig. 7 the calculations made in [10,11,50] are in reasonable agreement with ours for r^{04}_{00}, r^1_{1-1}, $\Im r^2_{1-1}$, $\Re r^5_{10}$, and $\Im r^6_{10}$ which are non-zero in the SCHC approximation. It is surprising that the solid and dash-dotted curves coincide practically with each other at $0.2 < Q^2 < 20\,\mathrm{GeV}^2$ for r^5 which is the greatest matrix element violating SCHC and proportional to the small spin-flip amplitude T_{01} ($\gamma^*_\mathrm{T} \to \varrho_\mathrm{L}$). For the quantity r^5, there is some difference between the dotted curve and the solid or dash-dotted curve, but all three calculations do not contradict the HERA data. Considering the description of r^1 and r^1_{11} we see that the difference between the Regge phenomenology prediction and the pQCD motivated calculations [10,11,50] is less than between the curves obtained in [10, 11, 50]. The last matrix element r^1_{11} in Fig. 7 is proportional to the small double spin-flip

amplitude $T_{1-1} = T_{-11}$, and hence gives the most direct information about its value. One can see that our calculations are in agreement with the data, while the calculations [10, 11] demonstrate probably some deviation from the ZEUS result at $Q^2 < 1\,\mathrm{GeV}^2$. The calculation of [50] gives zero for r^1_{11} since the double spin-flip amplitude T_{1-1} was put equal to zero.

We conclude from the comparison of different predictions for the spin density matrix that the difference between our results and the pQCD motivated calculations is of the same order of magnitude as the difference between those obtained in the perturbative QCD framework. Our calculations describe the high energy and high-Q^2 HERA data on the spin density matrix elements except r^{04}_{00} not worse than the pQCD motivated calculations. The Regge approach is more phenomenological and gives no fundamental information about the proton structure, but it can be used for relatively low energies where secondary reggeons contribute to the amplitude of the vector-meson leptoproduction. Our calculations can be useful for instance in the Monte Carlo estimations of relative contribution of the ϱ^0 meson production to semi-inclusive deep inelastic scattering.

4 Conclusions

The model for the description of the exclusive leptoproduction of ϱ mesons on nucleons has been considered. In this model, the virtual photon dissociation into the $q\bar{q}$ pair is described with the light-cone wave function, and the amplitude of scattering of the colorless $q\bar{q}$ system on the nucleon is calculated within Regge phenomenology. One, two, and three reggeon exchanges between the quark–antiquark pair and the nucleon have been taken into account. The parameters of the quark–reggeon vertices were obtained from those of the nucleon–reggeon vertices within the naive quark model. The parameters of the nucleon–reggeon vertices and the Regge trajectories were found in the seventies from an investigation of hadron–nucleon scattering at beam energies 10–100 GeV and $|t| \leq 0.5\,\mathrm{GeV}^2$. No free parameters have been used in the present calculations. The final state of the colorless $q\bar{q}$ pair is projected onto the state with $J^P = 1^-$ and isospin $I = 1$ to calculate the ϱ meson spin density matrix with the aid of the parton–hadron duality concept.

It is shown that the model works well at the total energy of the photon–nucleon scattering in the CM system $W > 4\,\mathrm{GeV}$, where the Regge phenomenology is known to be applicable. The calculations performed in the Regge approach are in reasonable agreement with the world data on the ratio $R = \sigma_\mathrm{L}/\sigma_\mathrm{T}$ (which is equivalent to the data on r^{04}_{00} in the SCHC approximation) at $Q^2 < 4\,\mathrm{GeV}^2$ where perturbative QCD is, strictly speaking, inapplicable. The present calculations of $\sigma_\mathrm{L}/\sigma_\mathrm{T}$ disagree with the available experimental data for $Q^2 > 4\,\mathrm{GeV}^2$ which are well described with pQCD. The Regge approach calculations of the spin density matrix elements r^a_{jk} other than r^{04}_{00} and the world data at $W > 4\,\mathrm{GeV}$ are in good agreement up to $Q^2 = 8\,\mathrm{GeV}^2$. The predictions of the present model agree unexpectedly well with the experimental data at the HERA collider energies for $0.5 < Q^2 < 20\,\mathrm{GeV}^2$. The difference between calculations of the spin density matrix in our approach and the pQCD motivated calculations is within the uncertainties of the theoretical results obtained in the perturbative QCD framework. The amplitudes computed in the Regge phenomenology approach do not conserve the S-channel helicity, but the parameters of the SCHC violation are small, their values being in reasonable agreement with the experimental data. The calculations of the SCHC violation parameters ξ_{10}, ξ_{01} in the perturbative QCD framework and in the Regge approach do not contradict each other. There is probably some disagreement between the two approaches for the case of the double spin-flip parameter ξ_{-11}.

Acknowledgements. I am grateful to J. Bartels for useful discussions and the hospitality. I am very much obliged to M.G. Ryskin for his constant interest in the present work and his valuable remarks and to A. Borissov who informed me about the new preliminary HERMES data. I would like to gratefully acknowledge also the hospitality of the DESY Theory Group. This work was supported by the NATO Collaborated Linkage Grant SA(PST.CLG.976453) 5437.

References

1. T.H. Bauer, R.D. Spital, D.R. Yennie, F.M. Pipkin, Rev. Mod. Phys. **50**, 261 (1978)
2. J.A. Crittenden, Springer Tracts in Modern Physics, Vol. 140 (Springer, Berlin, Heidelberg 1997)
3. M.G. Ryskin, Z. Phys. C **57**, 89 (1993)
4. S.J. Brodsky, L. Frankfurt, J.F. Gunion, A.H. Mueller, M. Strikman, Phys. Rev. D **50**, 3134 (1994)
5. A.D. Martin, M.G. Ryskin, T. Teubner, Phys. Rev. D **55**, 4329 (1997); D **62**, 014022 (2000)
6. J. Nemchik, N.N. Nikolaev, B.G. Zakharov, Phys. Lett. B **341**, 228 (1994)
7. D. Yu. Ivanov, R. Kirschner, Phys. Rev. D **58**, 114026 (1998)
8. M.G. Ryskin, Yad. Phys. **62**, 350 (1999) (Phys. Atom. Nucl. **62**, 315 (1999))
9. N.N. Nikolaev, Nucl. Phys. Proc. Suppl. **79**, 343 (1999)
10. N.N. Nikolaev, Acta. Phys. Polon. B **31**, 2485 (2000)
11. I.P. Ivanov, Ph.D. Thesis of Bonn university, Bonn, 2002, 172 p; hep-ph/0303053
12. C. Adloff et al., H1 Coll., Eur. Phys. J. C **13**, 371 (2000)
13. J. Breitweg et al., ZEUS Coll., Eur. Phys. J. C **6**, 603 (1999); C **12**, 393 (2000)
14. S.I. Manayenkov, Czech. J. Phys. 50, Supplement, S**1**, 117 (2000); DESY 99-016, 1999, unpublished; hep-ph/9903405
15. K.G. Boreskov, S.T. Sukhorukov, K.A. Ter-Martirosyan, Yad. Fiz. **21**, 825 (1975) (Sov. J. Nucl. Phys. **21**, 425 (1975))
16. K.G. Boreskov, A.M. Lapidus, S.T. Sukhorukov, K.A. Ter-Martirosyan, Nucl. Phys. B **40**, 307 (1972)
17. K.G. Boreskov, A.M. Lapidus, S.T. Sukhorukov, K.A. Ter-Martirosyan, Yad. Fiz. **14**, 814 (1971) (Sov. J. Nucl. Phys. **14**, 457 (1972))
18. N.I. Kochelev, Dong-Pil Min, Yongseok Oh, V. Vento, A.V. Vinnikov, Phys. Rev. D **61**, 094008 (2000)
19. S.J. Brodsky, G.P. Lepage, Phys. Rev. D **22**, 2157 (1980)

20. N.N. Nikolaev, B.G. Zakharov, Z. Phys. C **53**, 331 (1992)
21. J.B. Kogut, D.E. Soper, Phys. Rev. D **1**, 2901 (1970)
22. K. Schilling, G. Wolf, Nucl. Phys. B **61**, 381 (1973)
23. A.B. Kaidalov, Proceedings of the First ITEPh School on Physics, Elementary particles, vol. 2, p. 18 (Atomizdat, Moscow 1973)
24. G.L. Kane, A. Seidl, Rev. Mod. Phys. **48**, 309 (1976)
25. A.C. Irving, R.P. Worden, Phys. Rep. C **34**, 117 (1977)
26. K.A. Ter-Martirosyan, Yad. Fiz. **10**, 1047 (1969)
27. J.J.J. Kokkedee, The Quark Model, edited by W.A. Benjamin (New York 1969)
28. S. Aid et al., H1 Coll., Nucl. Phys. B **468**, 3 (1996)
29. A. Borissov, 10th Workshop on High-Energy Spin Physics: NATO Advanced Research Workshop, Nor-Amberd, Armenia, 30 June–3 July 2002, published in Nor-Amberd 2002, Spin Structure of Nucleon, p. 201; M. Tytgat, Ph.D. Thesis, Gent University (2001), DESY-THESIS-2001-018, April, 2001
30. J. Breitweg et al., ZEUS Coll., Eur. Phys. J. C **14**, 213 (2000)
31. V.B. Berestetsky, E.M. Lifshitz, L.P. Pitaevsky, Relativistic quantum theory, 2nd ed. (Nauka, Moscow 1968)
32. M. Derrick et al., ZEUS Coll., Phys. Lett. B **356**, 601 (1995)
33. M.R. Adams et al., E665 Coll., Z. Phys. C **74**, 237 (1997)
34. P. Amaudruz et al., NMC Coll., Z. Phys. C **54**, 239 (1992); M. Arneodo et al., Nucl. Phys. B **429**, 503 (1994)
35. C. del. Papa et al., Phys. Rev. D **19**, 1303 (1979)
36. A.D. Martin, R.G. Roberts, W.J. Stirling, R.S. Thorne, Eur. Phys. J. C **14**, 133 (2000)
37. H.L. Lai et al., Eur. Phys. J. C **12**, 375 (2000)
38. V. Eckardt et al., Nucl. Phys. B **55**, 45 (1973)
39. D.G. Cassel et al., Phys. Rev. D **24**, 2787 (1981)
40. J.T. Dakin et al., Phys. Rev. D **8**, 687 (1973)
41. J. Ballam et al., Phys. Rev. D **10**, 765 (1974)
42. P. Joos et al., Nucl. Phys. B **113**, 53 (1976)
43. J.J. Aubert et al., EMC Coll., Phys. Lett. B **161**, 203 (1985)
44. W.R. Francis et al., CHIO Coll., Phys. Rev. Lett. **38**, 633 (1977); W.D. Shambroom et al., CHIO Coll., Phys. Rev. D **26**, 1 (1982)
45. E.V. Kuraev, N.N. Nikolaev, B.G. Zakharov, Pis'ma v ZhETF **68**, 667 (1998) (JETP Lett. **68**, 696 (1998))
46. J.C. Collins, L. Frankfurt, M. Strikman, Phys. Rev D **56**, 2982 (1997)
47. A.D. Martin, R.G. Roberts, W.J. Stirling, Phys. Lett. B **387**, 419 (1996)
48. I.P. Ivanov, N.N. Nikolaev, Pis'ma v ZhETF **69**, 268 (1998) (JETP Lett. **69**, 294 (1999))
49. A. Ivanov, R. Kirschner, Eur. Phys. J. C **29**, 353 (2003)
50. I. Royen, Phys. Lett. B **513**, 337 (2001)